

INFN-14-08/LNF

1st April 2014

Electrons diffusion and signal noise contributions on electron clusters detection efficiency

M.Beretta, C.Gatti, G.Felici, G. Finocchiaro

INFN, Laboratori Nazionali di Frascati, P.O. Box 13, I-00044 Frascati

Abstract

The Cluster Counting (CC) technique, proposed for dE/dx measurements with the *SuperB* drift-chamber, could, significantly, improve particle identification by avoiding the fluctuations involved in charge measurements. As the technique is quite sensitive to the detector working conditions and to the front-end chain response, in this note we have investigated the effects on clusters detection efficiency of electron diffusion, preamplifier frequencyresponse and Signal-to-Noise Ratio (SNR) using different algorithms.

The evaluation is based on Garfield datasets, generated for a single cell geometry, at different impact points for $\pi/\mu/e$ particles with momenta 120, 140, 160, 180 and 210 MeV. The current waveforms generated by Garfield have been shaped according to the preamplifier response and different amounts of white gaussian noise has been added to the waveforms to simulate different SNRs. Finally an estimation of $\pi/\mu/e$ separation is shown.

Contents

1	Introduction	3
2	Garfield simulations	3
2.1	Cell geometry and working parameters	3
2.2	Gas properties	3
2.3	Simulation example	5
2.4	Time window optimization	5
3	Evaluation of Preamplifier Input Response	6
4	The Cluster Counting Algorithm	8
4.1	The Peak Detection Algorithms	8
4.2	The Slope Detection Algorithm	9
4.3	The Delay Line Algorithm	10
5	Convolution and Noise Effects on Detected Clusters	11
6	Cluster efficiency detection using the Delay Line algorithm	15
7	Clusters detection efficiency by means of the Delay Line algorithm using electrons, muons and pions data set at 0 mm impact point and different momenta	16
8	Conclusions	22

1 Introduction

The Cluster Counting (CC) technique for energy loss measurement was proposed in 1980 by Piuz and Lapique [1]. To investigate the feasibility of the technique we have generated five sets of orthogonal tracks crossing a 14 mm square drift tube filled with 90/10 *He/Is* gas mixture at 0 mm impact point from the wire for 120, 140, 160, 180 and 210 MeV $\pi/\mu/e$ particle momenta.

The output waveforms have been convolved with the preamplifier impulse response and different amount of white gaussian noise has been added to the convolved waveforms to evaluate the noise sensitivity of the used algorithms.

Furthermore the influence of electrons diffusion on cluster reconstruction efficiency has been investigated using different time integration windows.

2 Garfield simulations

2.1 Cell geometry and working parameters

The simplified 1.4 cm square tube geometry, shown in figure 1, has been used to simplify simulations. The selected working parameters are shown in table 1.

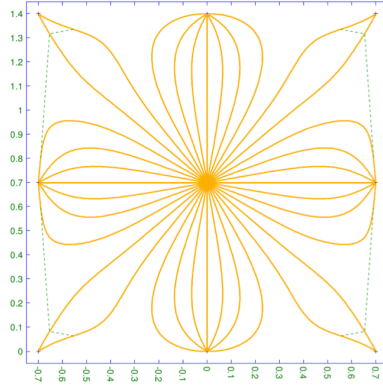


Figure 1: Cell geometry and isochrones used in Garfield simulation

2.2 Gas properties

The simulation results of the gas mixture properties are shown in figure 2. An electron mean free path of about 770 μm corresponding to about 13 clusters/cm with an average cluster size of about 1.3 e/cluster can be inferred from plots a) and b). The c) and d) plots

Table 1: Garfield working conditions

Voltage (sense wire)	1850V
Magnetic field	0
Gas Mixture	He (90%) Iso (10%)
Ion mobility	10.4 [cm^2/Vs]
Gas amplification	$18 \cdot 10^4$ (Polya distribution with $\theta=0.6$)

show the gas mixture behavior in terms of diffusion and drift velocity. As an example from plot d) an electric field of about $3 \cdot 10^4$ V/cm corresponds to a drift velocity of $40 \mu m/ns$ then a time window of 5 ns could be used, as shown in plot c), to compensate for the $200 \mu m$ diffusion.

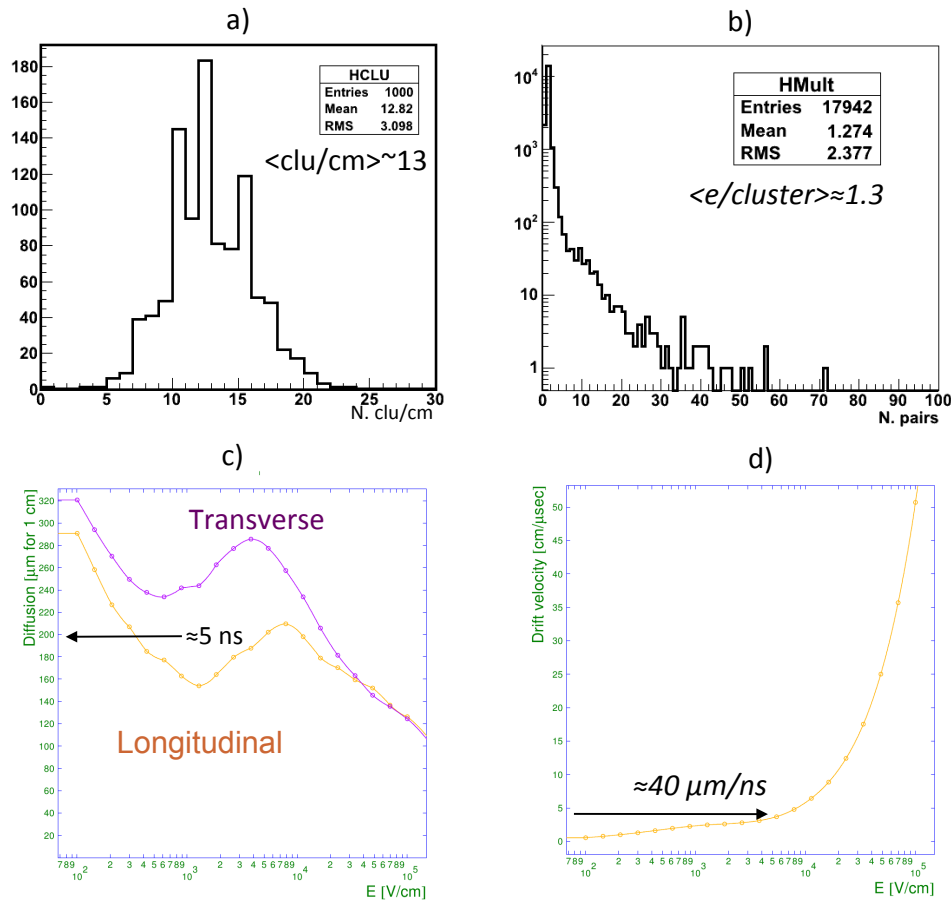


Figure 2: Gas properties (from simulations): a) number of clusters per cm, b) cluster size, c) diffusion, d) drift velocity.

The mean number of clusters produced by electron, muon and pions in a 14 mm cell is shown in figure 3 as a function of the particle momentum. Electrons and muons overlap for $p = 140$ MeV/c while electrons and pions overlap for $p = 180$ MeV/c.

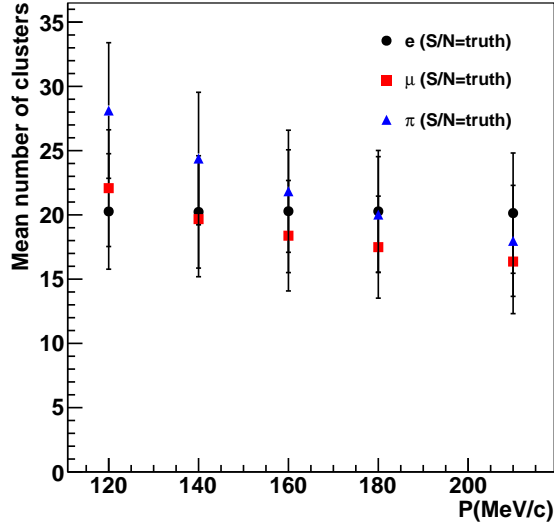


Figure 3: Mean number of clusters produced in a 14 mm cell as a function of momentum for electrons, muons and pions. The markers represent the mean number of produced clusters while the error bars represent the distribution standard-deviation.

2.3 Simulation example

An example of simulation output is shown in figure 4 where both the particle track at 2 mm impact parameter and the corresponding output-current signal are shown.

2.4 Time window optimization

If the correct number of clusters generated from a crossing particle must be detected the effect of diffusion must be taken into account. This is clearly visible in figure 5 where 1 ns integration time has been used. Electrons belonging to a single cluster split up by diffusion process and are counted as single-electron clusters. This effect is partially compensated increasing the integration time as shown in figure 6 where the cluster-detection efficiency has been plotted as a function of the integration time for different impact points. Low integration time causes extra counting due to the splitting-up effect, while excessively high integration time causes inefficiency due to the cluster merging.

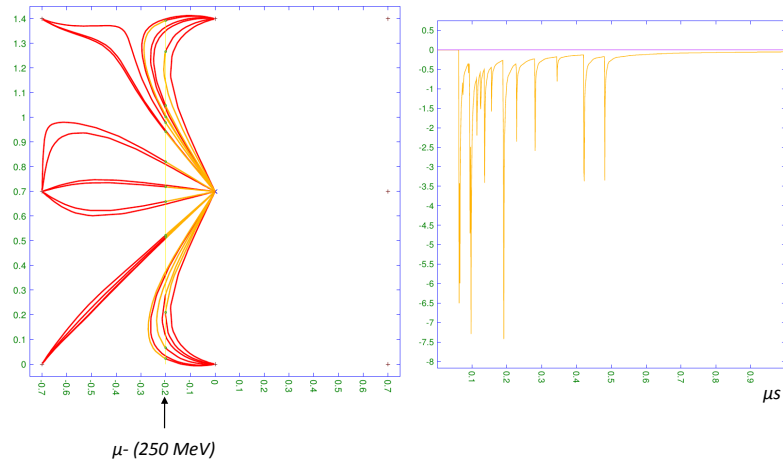


Figure 4: Simulation example: a) orthogonal track at 2 mm from wire and b) corresponding output current signal

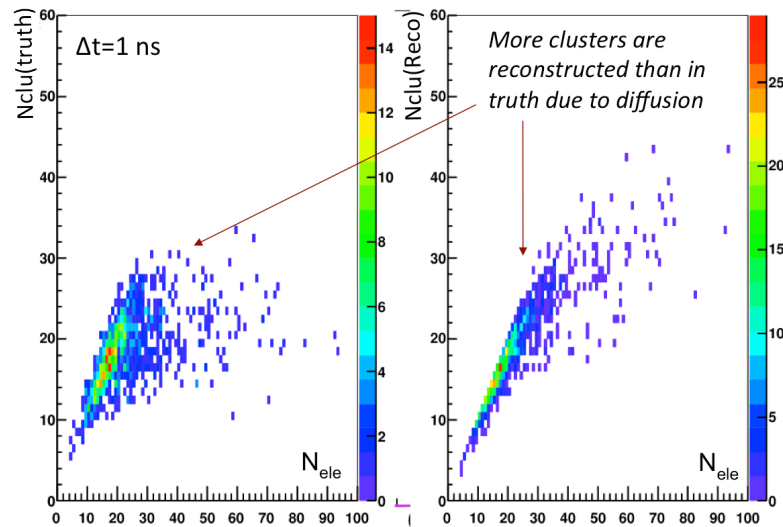


Figure 5: Detected number of clusters with 1 ns integration time as a function of the generated number of electrons. Left: truly generated clusters. Right: number of reconstructed clusters.

3 Evaluation of Preamplifier Input Response

To evaluate the effect of the preamplifier bandwidth on the sense-wire current signal we have parametrized the response of the front-end used to instrument the Superb DCH pro-

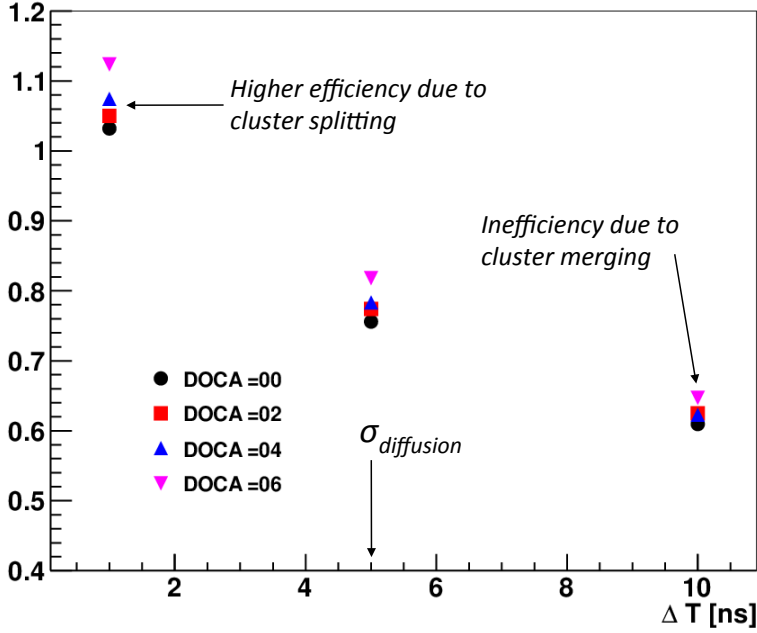


Figure 6: Reconstructed clusters versus integration time

totypes. The preamplifier is based on a transresistance configuration and its main features are shown in Table 2.

To investigate the preamplifier impulse response we have injected a δ -like pulse to the

Table 2: Preamplifier main specifications

Linearity	$< 1\%(1 - 100fC)$
Gain	$\sim 8.8 \text{ mV/fC}$
Z_{IN}	60Ω
Z_{OUT}	50Ω
Rise time	$\sim 2.4 \text{ ns } (C_D = 24pF)$
Fall time	$\sim 2.4 \text{ ns } (C_D = 24pF)$
Noise	$3000 \text{ erms } (C_D = 24pF)$
V_{SUPPLY}	$\pm 6V$

preamplifier input and acquired the output by means of a 4 GSamples/s digital scope. The preamplifier was connected to one of the 2.7 m length prototype sense wires. Both test pulse and preamplifier output digitized waveforms are shown in figure 7. The digitized signal has been fitted with a double gaussian function, equation 1, then obtaining

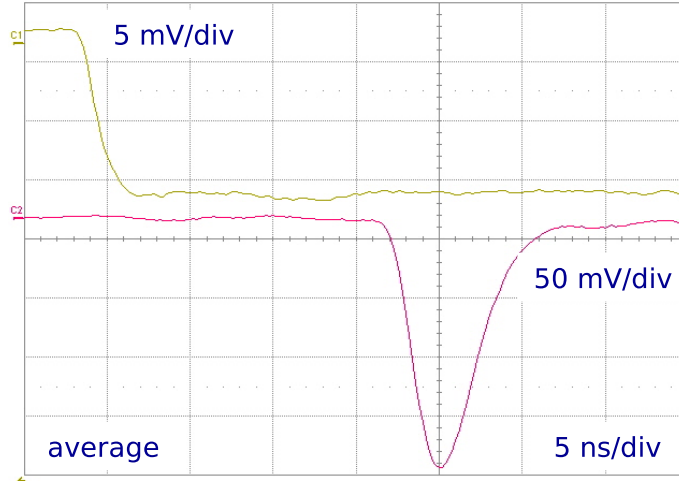


Figure 7: Preamplifier response (1.8 pF injecting capacitance).

the parameters of table 3. The result of the fit is shown in figure 8.

$$h(t) = a_1 e^{-\left(\frac{t-b_1}{c_1}\right)^2} + a_2 e^{-\left(\frac{t-b_2}{c_2}\right)^2} \quad (1)$$

Table 3: Fitting function coefficients

a_1	0.479
b_1	24.367
c_1	1.797
a_2	0.691
b_2	25.983
c_2	2.305

4 The Cluster Counting Algorithm

Three different Cluster Counting algorithms have been evaluated: Peak Detection, Slope Detection and Delay Line. The algorithms are shortly discussed in the following.

4.1 The Peak Detection Algorithms

The Peak Detection (PD) algorithm is the simplest (and faster) CC algorithm. It is based on different time data samples comparison. The working principle of PD algorithm is

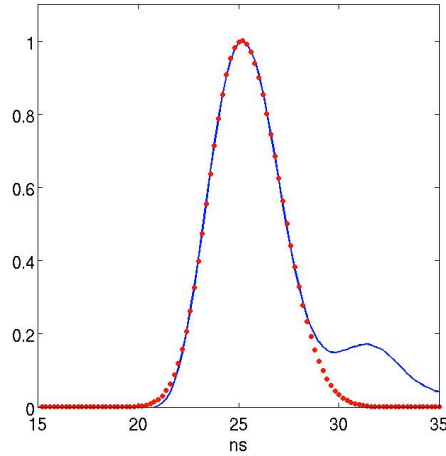


Figure 8: Preamplifier impulse response (line) and fittings (dotted line).

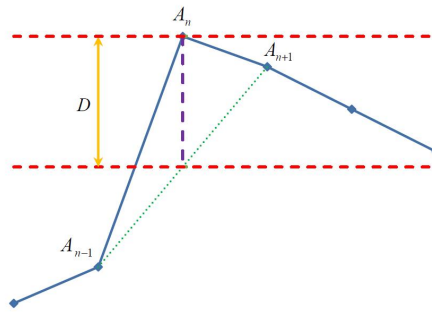


Figure 9: Peak Detection working principle.

shown in figure 9, while equation 2 shows the algorithm used in our simulation.

$$| A_n | > (| A_{nx} | + \sigma) \ \&\& \ | A_n | > (| A_{ny} | + \sigma) \quad (2)$$

where A_{nx} , A_n and A_{ny} are three increasing data samples while σ is the noise (rms) evaluated when no signal is present.

4.2 The Slope Detection Algorithm

The Slope Detection algorithm is based on the detection of signal rising (or falling) slope. The slope is evaluated as the difference between a sampling and the average of preceding ones (figure 10). A slope change occurs when the comparison implemented on three (or more) consecutive samplings comes true with respect to a fixed threshold value. Once a

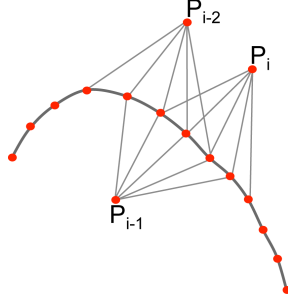


Figure 10: Slope detection working principle.

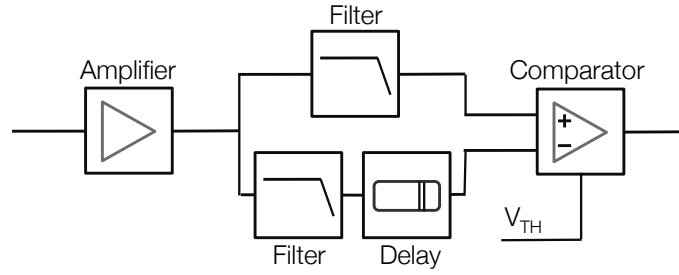


Figure 11: Delay Line working principle.

slope change is detected a dead time is asserted to avoid extra counting.

$$P_i = A_i - \frac{\sum_{n=1}^4 A_{i-n}}{4} \quad (3)$$

$$C_1 = P_i - P_{i-1} \quad C_2 = P_{i-1} - P_{i-2} \quad C_3 = P_i - P_{i-2} \quad (4)$$

$$(C_1 < -Thr) \text{ AND } (C_2 < -Thr) \text{ AND } (C_3 < -Thr) \quad (5)$$

where A_i are the data samples and Thr is the threshold.

4.3 The Delay Line Algorithm

Both the previous algorithms require fast digitizer (at least 1 GSPS FADC) and state of art FPGA to be implemented in a measurement system. On the contrary the Delay-Line algorithm hardware can be easily implemented as shown in figure 11. The circuit, essentially, compares a delayed copy of the signal with a bandwidth limited copy of the signal itself.

5 Convolution and Noise Effects on Detected Clusters

There are two main contributions to cluster detection inefficiency: the preamplifier bandwidth and the front-end noise. The effect of preamplifier bandwidth is shown in figure 12

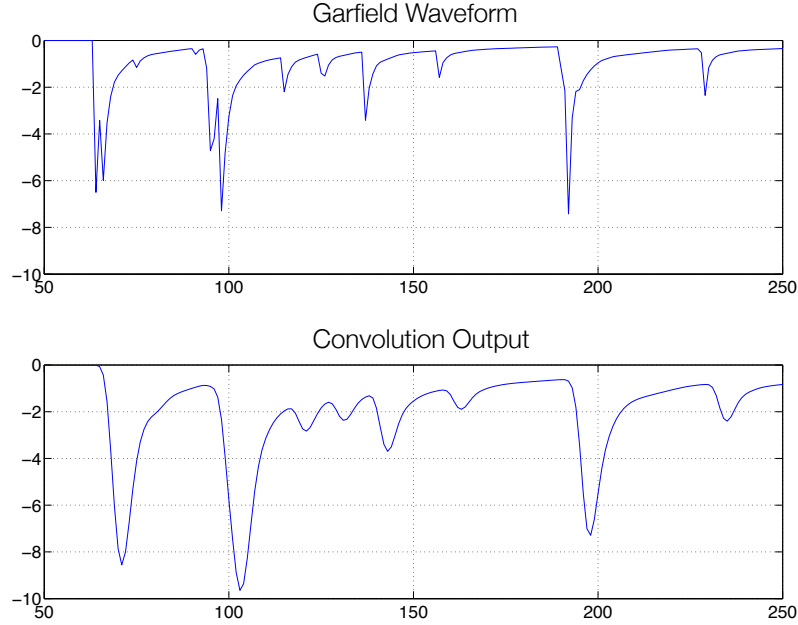


Figure 12: Example of the convolution effects on a single waveform.

where the pure Garfield signal is convolved with the preamplifier response. Because of the preamplifier limited bandwidth different clusters are merged in a single one, then reducing the detection efficiency.

Concerning the electronic noise, if we discard the contribution of external interferences, the front-end chain noise contribution can be estimated generating waveforms with different Signal to Noise Ratio (SNR) according to equation 6).

$$SNR = \frac{\text{signal average}}{\text{standard deviation}} \quad (6)$$

In equation 6 the *signal average* corresponds to the single electron cluster average amplitude that can be inferred from the average cluster amplitude and the average cluster size. The average cluster size measurement has been carried out by evaluating, for each cluster, the absolute value of cluster amplitude and the absolute value of the same cluster starting point within each waveform. The difference in amplitude of the two measures is stored in a vector and, finally, the cluster average amplitude is calculated for all waveforms. The

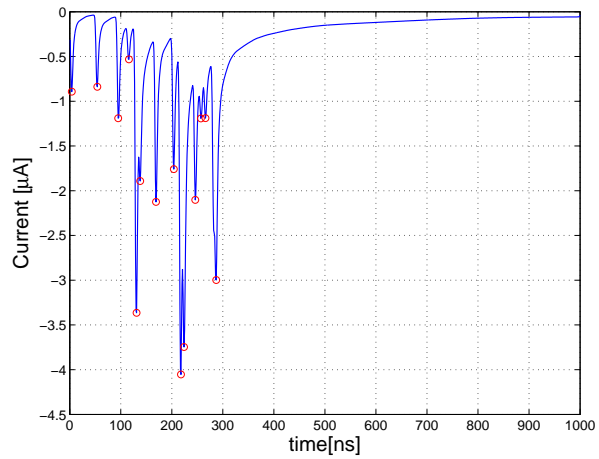


Figure 13: Example of clusters used for the average amplitude calculation

average cluster amplitude for each particle and momenta at 0 mm impact point is shown in table 4, while an example of the detected clusters is shown in figure 13.

From table 4 the average current for single-electron cluster have been evaluated dividing the currents by 1.33 (the used gas mixture average cluster size). The value obtained has been then used to add noise to the waveforms according to equation 6 as shown in figure 14.

To estimate the inefficiency contributions four different data sets have been considered (as an example) for 120 MeV electrons at 0 mm impact point:

- first data set: the original Garfield waveforms;

Table 4: Average clusters peak current (μA) - $I_{peak\ ave} \pm I_{peak\ rms}$

MeV	electrons	μ^-	π^-
120	1.67 ± 1.83	1.76 ± 1.99	1.84 ± 2.11
140	1.68 ± 1.84	1.73 ± 1.99	1.78 ± 1.97
160	1.68 ± 1.87	1.73 ± 2.11	1.76 ± 1.93
180	1.66 ± 1.79	1.69 ± 1.82	1.74 ± 2.02
210	1.68 ± 1.80	1.69 ± 1.96	1.68 ± 1.89

Table 5: Inefficiency contribution evaluated using 120 MeV electrons (IP = 0 mm) and the Peak Detecting algorithms

Data	Efficiency
Garfield Waveforms	1
Garfield Waveforms + Convolution	0.75 ± 0.10
Garfield Waveforms + Noise (SNR = 12)	0.81 ± 0.10
Garfield Waveforms + Convolution + Noise (SNR = 12)	0.55 ± 0.11

- second data set: the Garfield waveforms convolved with preamplifier response;
- third data set: the Garfield waveforms with white gaussian noise corresponding to a SRN=12;
- fourth data set: the convolved waveforms with gaussian noise corresponding to a SNR=12;

The simple "Peak Detecting" algorithm has been used to detect clusters. Results are shown in table 5. Both the noise and the convolution, when considered separately, give a contribution of the order of 20-25% to inefficiency. The inefficiency contribution increases to about 50 % when the contribution of both effects is considered¹.

A more systematic study of detection efficiency has been carried out using the Delay Line algorithm. This algorithm has been chosen as it can be easily hardware implemented with respect to the Peak Detecting and Slope Detection ones that require fast and expensive digitizing devices.

¹To evaluate the contributions of preamplifier shaping time, noise and shaping time + noise we have assumed the Garfield generated waveforms efficiency equal to 1

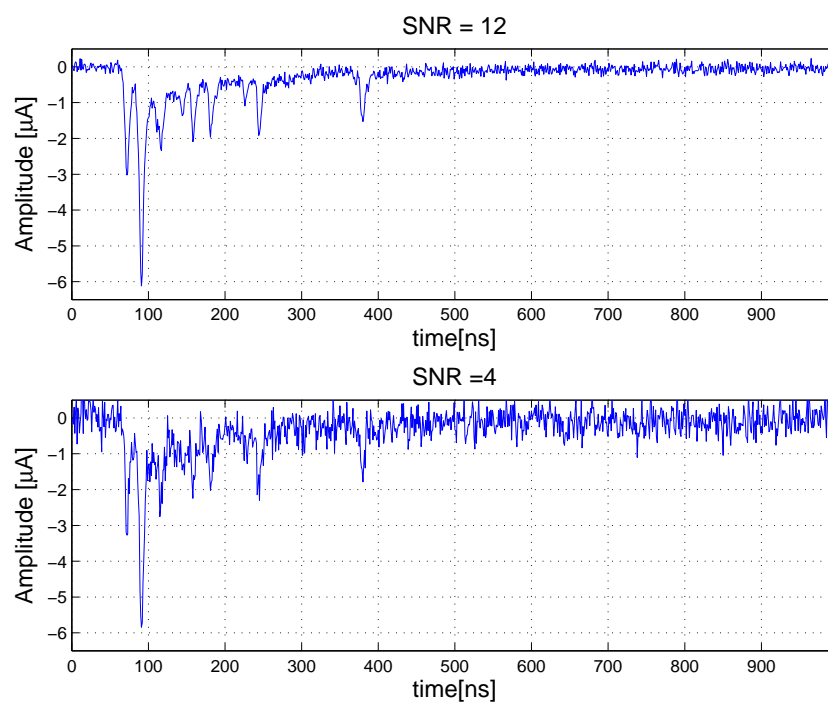


Figure 14: Garfield waveforms with different levels of added noise.

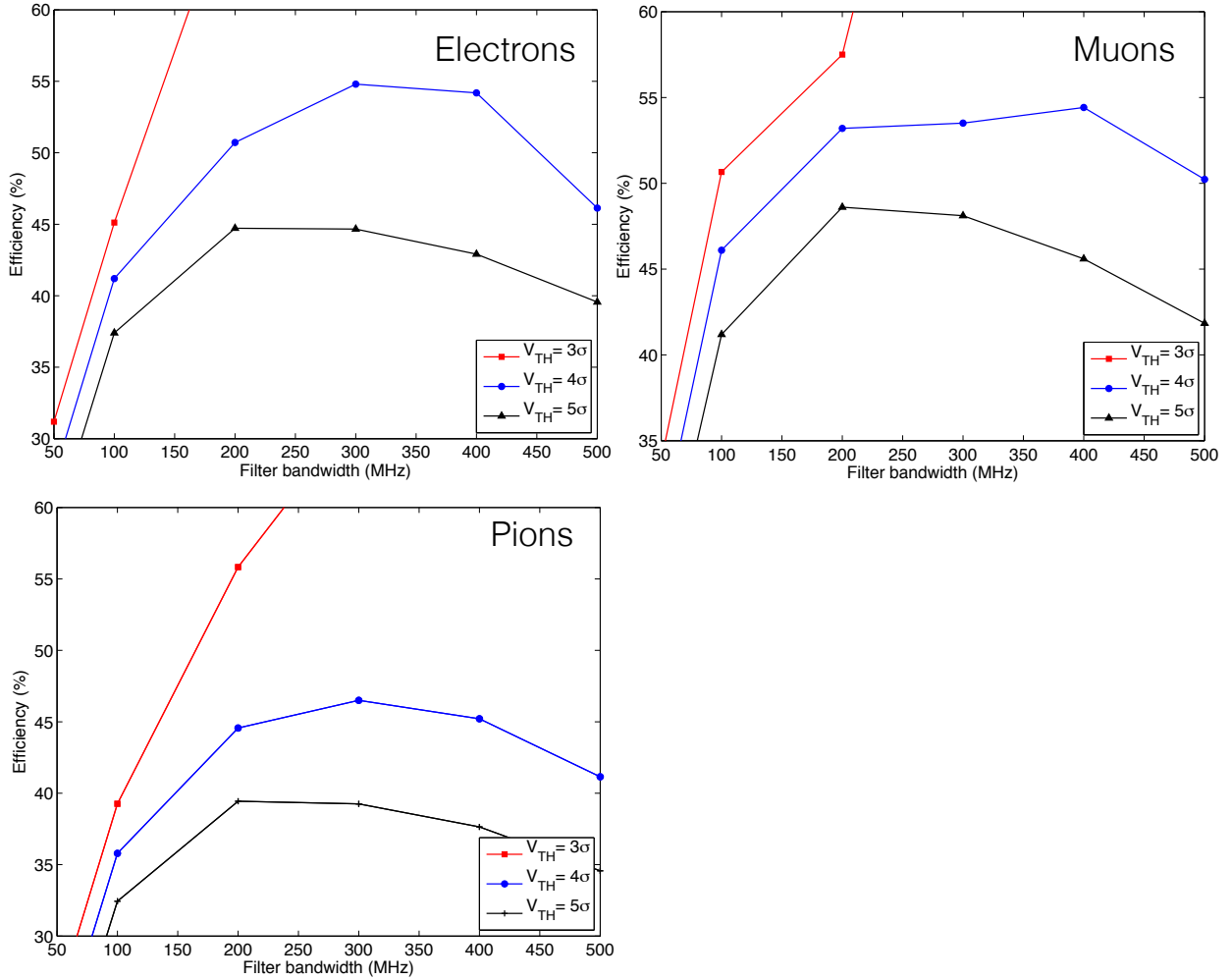


Figure 15: Efficiency scan carried out on 120 MeV electrons, muons and pions at 0 impact point data set (SNR=12) as a function of filter bandwidth for different thresholds.

6 Cluster efficiency detection using the Delay Line algorithm

The Delay Line algorithm makes use of three parameters: the LP filter bandwidth, the signal delay and the discriminator threshold. As the three parameters are correlated, the efficiency behavior as a function of the frequency filter has been investigated, at fixed delay, for different thresholds using the 120 MeV electrons, muons and pions data at SNR=12 and 0 mm impact point; the delay has been set to 3 ns (compatible with preamplifier shaping time). The thresholds have been set to a multiple of the noise standard-deviation (σ) in the *filtered* signal. The results, shown in the plot of figure 15, suggest the use of a 300

MHz LP filter together with a threshold of 4σ as best compromise between bandwidth, threshold and safe working conditions (no ghost counts). In detail plots of figure 15 show that:

- using a 3σ threshold the counting is dominated by noise for filter bandwidth exceeding 150-200 MHz;
- 4σ is a safe threshold value (no ghost counts neglecting the muons small counting increase for high bandwidth);
- efficiency decrease for bandwidth higher than 250-300 MHz is due to the increase ² of evaluated σ .

Finally, to select the right delay, an efficiency scan over different values has been carried out. The scan results, shown in figure 16, point out that the efficiency detection for electrons, muons and pions is maximized setting a delay of 3 ns, that is a value compatible with the preamplifier shaping time (figure 7).

Summarizing, the plots confirm that 300 MHz bandwidth filter and 3 ns delay together with a 4σ filter are the parameters that maximize the cluster-detection efficiency.

7 Clusters detection efficiency by means of the Delay Line algorithm using electrons, muons and pions data set at 0 mm impact point and different momenta

A scan over different momenta at 0 mm impact point has been carried out using the parameters previously defined. The Delay-Line algorithm is used, as described above, to the simulated data after applying different amount of white noise. The effect of the noise on the mean number of observed clusters as a function of the particle momentum is shown in figure 17. In this momentum region, signal from different particles are separated at most by about one standard deviation. The separation is worsened as the amount of noise is increased. Examples of distributions of number of detected clusters are shown in the lower plots of figure 19. The distributions, obtained for different levels of noise, are almost gaussian, showing the (expected) absence of any long tail that would spoil the performance of particle identification.

The cluster detection efficiency is obtained by dividing for the produced number of clusters shown in figure 3. The result is shown in figure 18 for electron, muon and pions separately, as a function of the signal-to-noise ratio, including the *ideal* case when no

²For each bandwidth point, the standard deviation of the *filtered* signal is evaluated in a section of the waveform where there is no signal

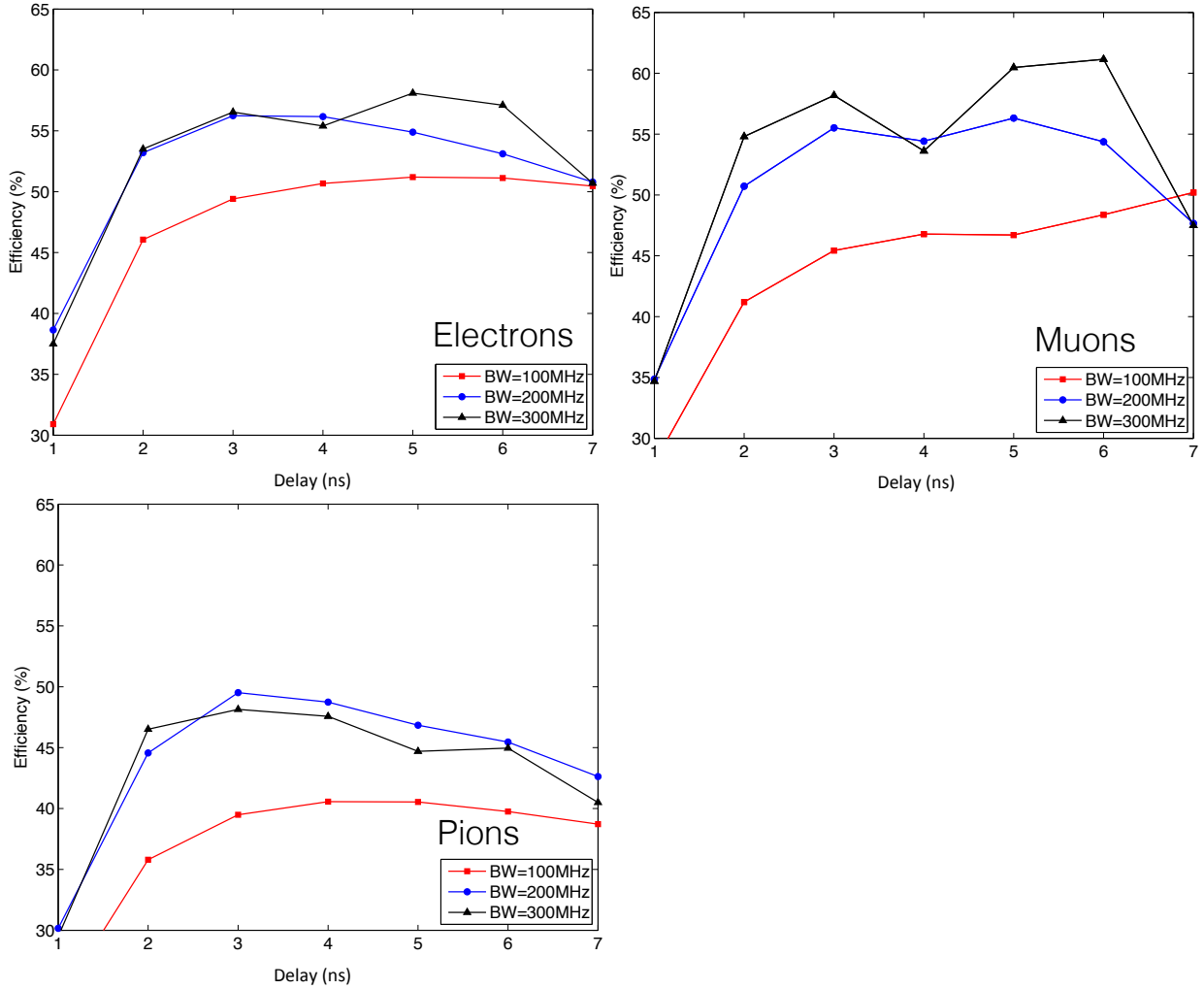


Figure 16: Efficiency scan carried out on 120 MeV electrons, muons and pions at 0 mm impact point data set ($SNR=12$, Threshold = 4σ) as a function of applied delay for different bandwidth (efficiency raise for delay greater than 4 ns is due to the detection of signals over-hreshold belonging to different peaks).

noise is included and only the convolution with the preamplifier response is considered. The statistical error is smaller than the marker size and is not visible. For $S/N = 12$ we observe an efficiency value between 50 and 60% for all particles and momenta. As explained in the previous section, this is due both to the noise and to the convolution with the preamplifier response. For $S/N < 8$ the efficiency drops down well below 50%.

In the ideal case, we observe an efficiency of about 90%; We note that this value is the same for electrons independently of the momentum, while there is a clear correlation

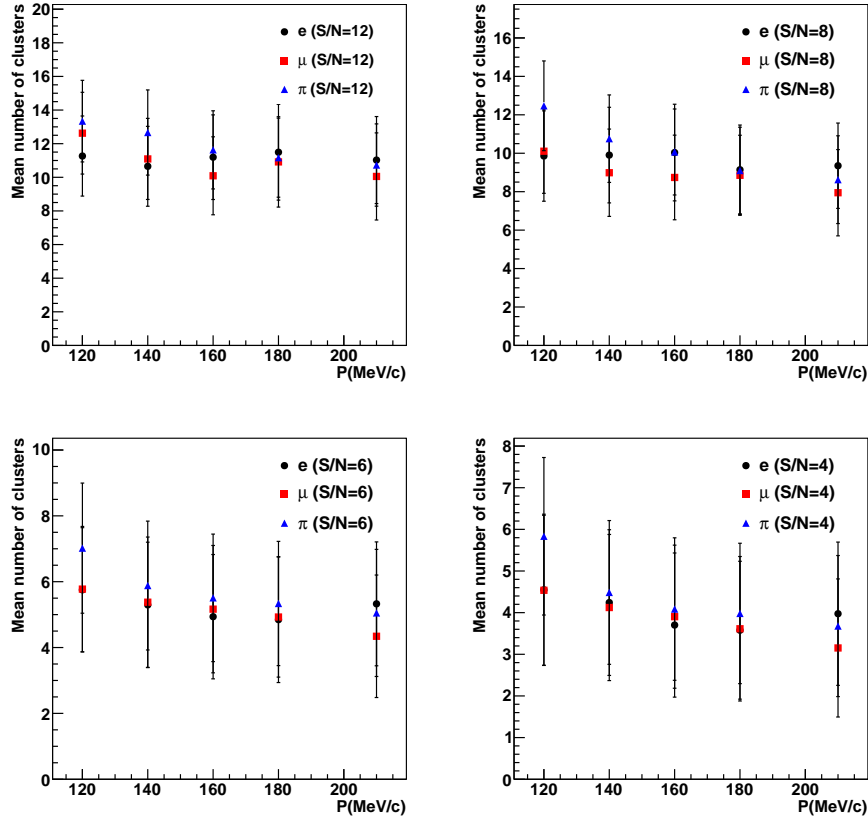


Figure 17: Mean number of detected clusters as a function of momentum for electrons, muons and pions, for simulations with different amount of white noise. The markers represent the mean number of detected clusters while the error bars represent the distribution standard-deviation.

between efficiency and momenta for pions and muons: the efficiency increases with increasing momentum. This can be understood by looking at figure 3. Electrons produce the same number of clusters in 14 mm (about 20) independently of their momentum. Therefore, the ionization length is constant, about $700 \mu\text{m}$, and so is the probability for a cluster to be so close in time to a previous cluster to be missed by our algorithm. Figure 15, for instance, shows the correlation between dead-time ($1/\text{bandwidth}$) and efficiency. The situation is different for pions and muons. Pions, for instance, produce about 30 clusters in 14 mm at 100 MeV/c and about 20 clusters at 210 MeV/c. The ionization length increases by a factor $3/2$, approximately, and the efficiency increases accordingly. Since muons and electrons with about 140 MeV/c momentum produce the same number of clusters, we expect the efficiencies for these two particles to be similar at this value of the momentum.

Similarly, pions and electrons produce the same number of clusters for momenta close to 180 MeV/c, and so also the efficiencies should be similar. This is, more or less, confirmed by the *ideal* points in figure 18.

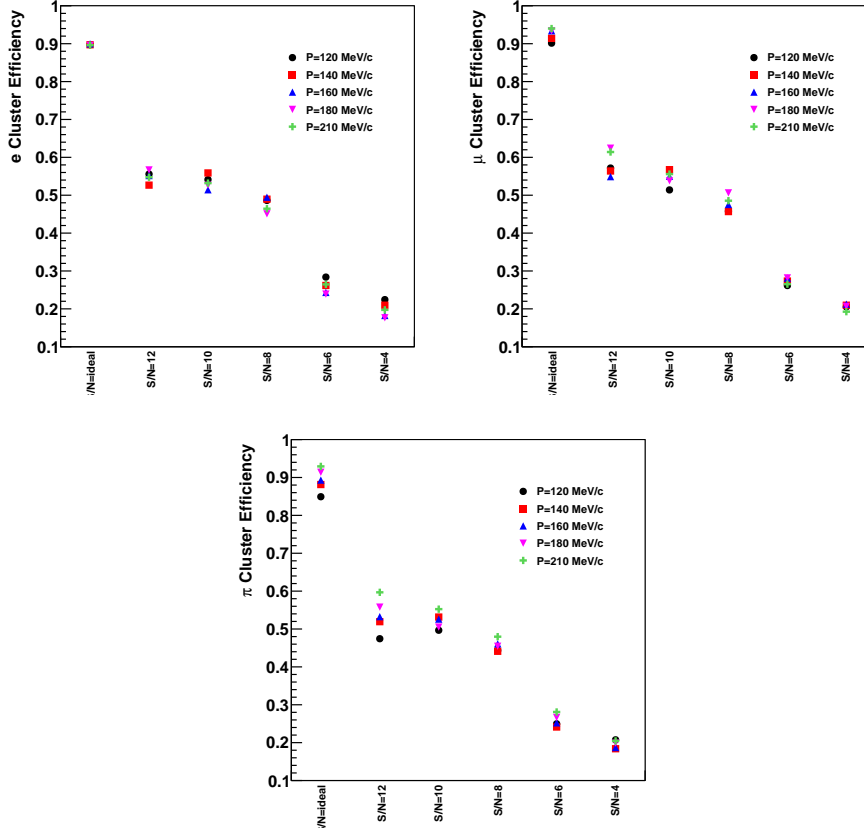


Figure 18: Cluster detection efficiency as a function of the signal-to-noise ratio for electrons, muons and pions. In the *ideal* case, only the convolution with the preamplifier response function is considered (no white noise is applied).

The rejection-efficiency curves (ROCs) for the separation of electrons and pions, with a single cell of 1.4 cm, are shown in figure 19 at 120 MeV momentum for three values of the signal to noise ratio. The rejection and selection probabilities are obtained by simply counting the fraction of events with a number of clusters above or below a given threshold. By varying this threshold we obtain from the distribution shown in the lower plots in figure 19 the curves shown in the upper plots. For instance, for $S/N = 10$ there is a clear separation between the number of clusters of pions and electrons. This results in a ROC more similar to a quarter of circle (with integral $\sim \pi/4$). Increasing the

amount of noise, the ROCs become similar to the anti-diagonal (integral 0.5), meaning no discrimination power between the two hypotheses.

The same distributions are shown for electron-muon separation in figure 20.

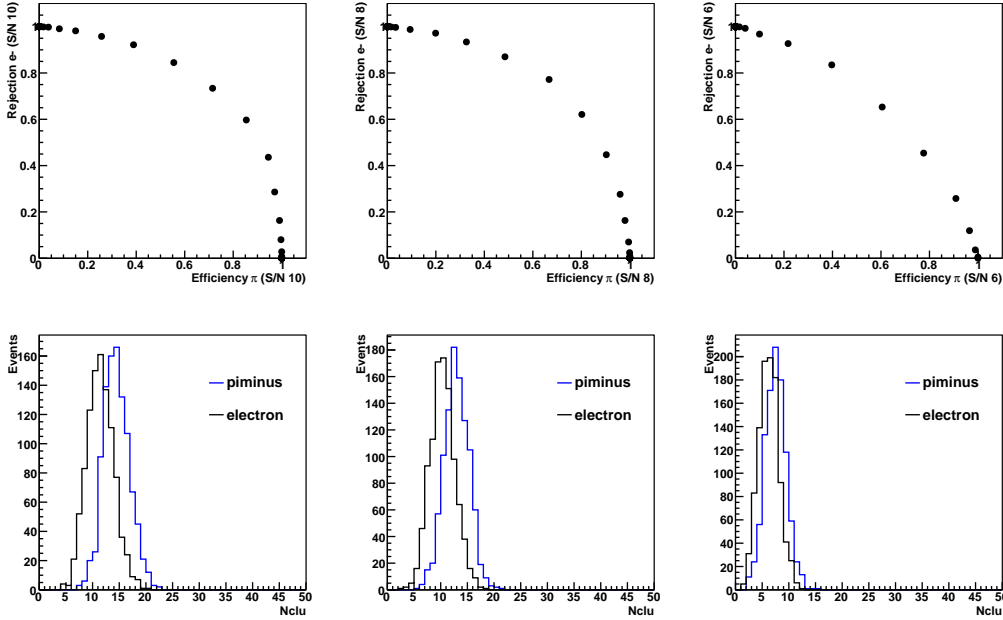


Figure 19: Rejection-efficiency curves with a single 1.4 cm cell for the electron-pion separation at 120 MeV and for three different levels of noise. In the lower plots we show the corresponding cluster distributions from which the efficiencies are calculated.

These ROCs are shown for a single cell. An estimate of the performance achievable with more cells can be estimated using binomial probability distribution. If ϵ is the efficiency for the signal and $1 - r$ the efficiency for the background, the expected separation in the number of crossed cells with a *good* or *bad* signal, in standard deviation units, is given by:

$$\frac{\Delta N}{\sigma} = \frac{N_{signal} - N_{bkg}}{\sigma_{signal} \oplus \sigma_{bkg}} = \sqrt{N_{cell}} \frac{\epsilon + r - 1}{\sqrt{\epsilon(1 - \epsilon) + r(1 - r)}} \quad (7)$$

So, for instance, for $e - \pi$ separation at $120 MeV/c$ and $S/N=10$, if we consider the point with $\epsilon \simeq r \simeq 0.7$ we expect with $N_{cell} = 40$ a separation of about 4 standard deviations between electron and pion average signals. In the worst case of $\epsilon \simeq r \simeq 0.6$ and $N_{cell} = 40$, we expect a separation of about 2 standard deviations.

As anticipated, the ROC separation-power can be summarized by its integral. The maximal separation is achieved when the integral is 1 (or 0) and no separation is achieved

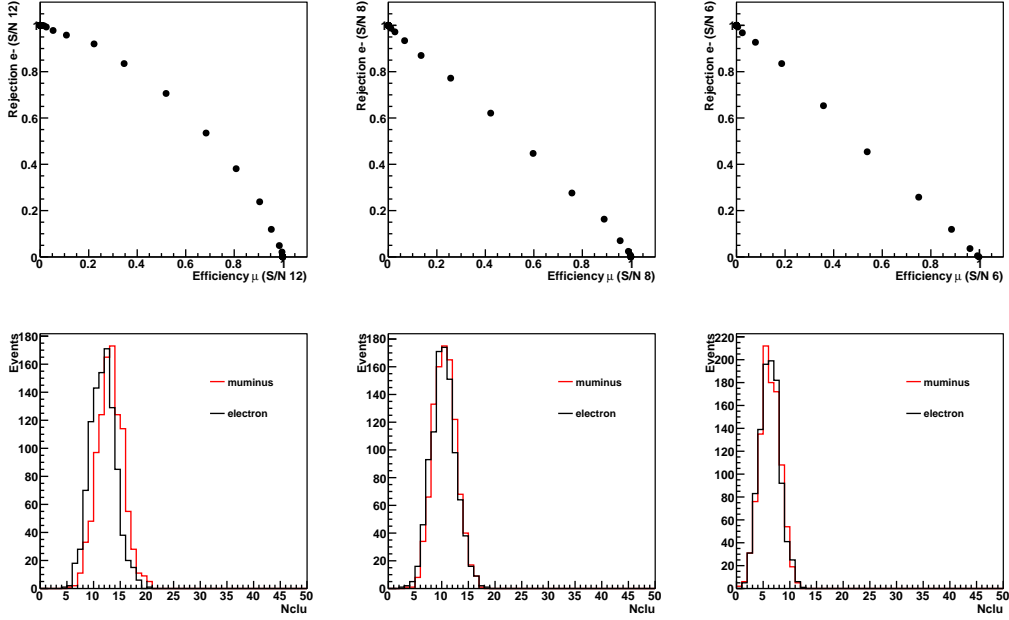


Figure 20: Rejection-efficiency curves with a single 1.4cm cell for the electron-muon separation at 120 MeV and for three different levels of noise. In the lower plots we show the corresponding cluster distributions from which the efficiencies are calculated.

when the ROC integral is equal to 0.5. The ROC integrals for all particles and different momenta as a function of the noise level are shown in figure 21. A value of the integral less than 0.5 simply means that the meaning of rejection and efficiency have to be inverted. This happens for instance for electrons at higher momenta when their ionization is larger than that of muons and pions.

Particle separation can be performed for all momentum values but for those where the ionization of the two particle species is the same (e.g. 140 MeV/c for electrons and muons and 180 MeV/c for electrons and pions). As the noise increases, the points tend to cluster close to the value 0.5 indicating that particle identification becomes more and more difficult.

Finally, the values of $\Delta N/\sigma$ defined in equation 7 for different particle hypotheses are shown in figure 22 as a function of the momentum in the case of $N_{cell} = 40$ and $S/N=12$.

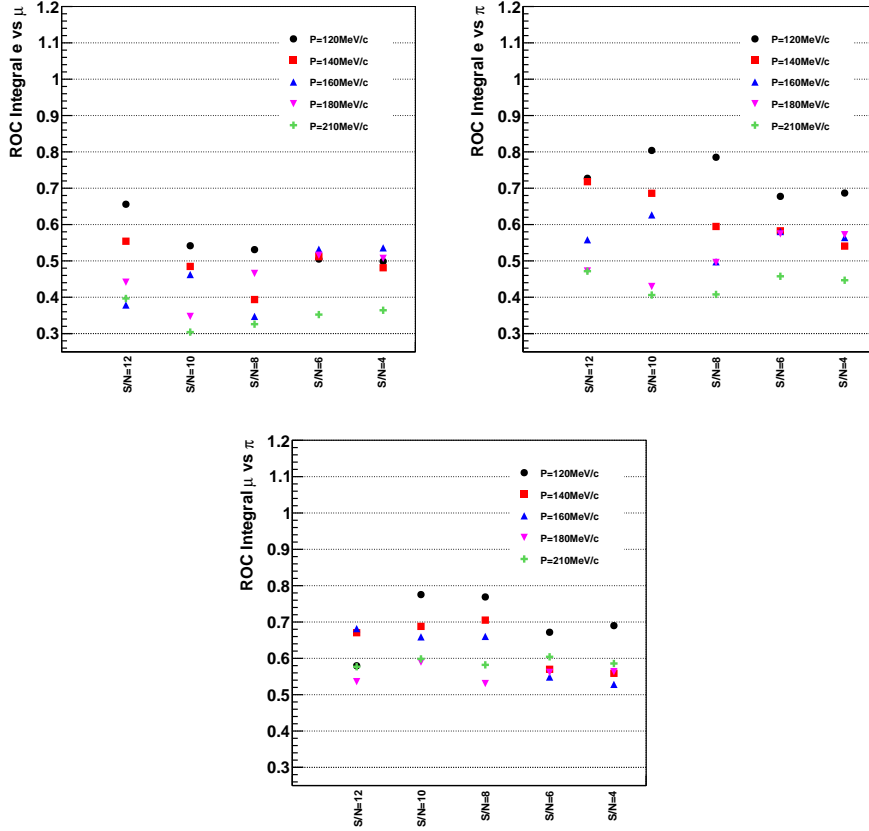


Figure 21: ROC integrals for the electron-muon, electron-pion and muon-pion separation for different momenta and for different levels of noise.

8 Conclusions

The Cluster-Counting technique can significantly improve particle identification avoiding fluctuations involved in charge measurement. Using events simulated with Garfield combined with a parametrization of the preamplifier response, we have investigated the best working point and performance for a delay-line algorithm. We find that both the inverse of the filter band-width and delay time must be of the order of the width of the preamplifier response (about ~ 3 ns) to maximize cluster detection efficiency and the signal threshold must be set to about four noise standard-deviations. With these values, the cluster detection efficiency is about 50% when the signal-to-noise ratio is 12, and rapidly deteriorates to 20% as the signal-to-noise ratio is lowered to 4. Also the discrimination power worsen as the level of noise is increased. For S/N=12 and considering a drift chamber with 40 cells of 1.4 cm, about 1 sigma separation is possible for all particle hypotheses in almost

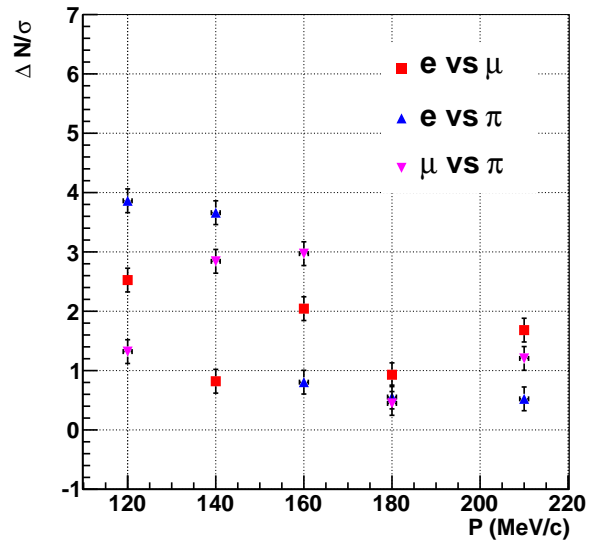


Figure 22: Variable $\Delta N/\sigma$ defined in equation 7 for different particle hypotheses for $N_{cell} = 40$ and $S/N=12$.

all the momentum-range considered. The worst separation is achieved for momenta equal to 180 MeV/c.

References

- [1] F. Lapique and E. Piuz, Simulation of the measurement by primary cluster counting of the energy lost by a relativistic ionizing particle in argon, Nucl. In. and Meth. 175 (1980) 315.